The International Journal of Advanced Manufacturing Technology (2018) 97:3395–3405
https://doi.org/10.1007/s00170-018-2118-3

ORIGINAL ARTICLE

Effect of temporal control of air/water environment on laser drilling of nickel-based alloy with thermal barrier coatings

Zhaoyang Zhai [1,2,3] · Wenjun Wang [1,2,3] · Xuesong Mei [1,2,3] · Kedian Wang [1,2,3] · Fangcheng Wang [1,2,3] · Aifei Pan [1,2,3]

Received: 17 October 2017 / Accepted: 6 May 2018 / Published online: 25 May 2018

Abstract

This study adopted nanosecond laser to conduct drilling research on nickel-based alloy with thermal barrier coatings (TBCs). The experiments of different processing environments on quality and efficiency of laser drilling were conducted. Through combination of high processing efficiency under air environment and good processing quality under water environment, temporal control of air/water environment on laser drilling is proposed. Since drilling efficiency was not significantly reduced, cold machining effect of water was used to improve processing quality. Research results proved that laser processing method with temporal control of air/water environment has advantages of traditional laser drilling under air and water. Laser drilling of temporal control of air/water environment was improved in quality in comparison with single environment.

Keywords Nickel-based alloy · Thermal barrier coatings · Laser drilling · Processing environment · Temporal control

1 Introduction

The evolution of aero-engine affects directly the promotion of airplane performance. Specifically, the military aero-engine presents greater thrust-weight ratio, higher turbine forward temperature, and many other preferable technical characteristics. To ensure turbine blade reliable operation under high temperature, single-crystal nickel-based alloys were used as a turbine blade material and film cooling is usually adopted to cooperate with thermal barrier coating. Since hard materials are used for blades and the film cooling holes are small, non-traditional machining methods are usually adopted to fabricate the cooling holes at present. Such techniques are electro discharge machining (EDM) [1], electrochemical machining (ECM) [2], and laser drilling [3]. Among these processing technologies [4], laser processing has several advantages such as high efficiency, good quality, non-contact processing, and low heat input. In addition, it is easy to combine with a numerical control (NC) technique to realize automation and it can finish processing of cooling holes on blade with thermal barrier coatings (TBCs) in one-step process. Consequently, laser drilling has a prospect to become the main processing technology of film cooling holes on turbine blade in the future.

For laser processing of film cooling holes, some researchers used a high-power and long-pulse laser to achieve high efficiency but thick recast layer would form inside the holes with a large quantity of microcracks [5], seriously affecting service performance of blade. Chien et al. [6] selected Inconel 718 to carry out Nd:YAG laser drilling experiments. They found that holes drilled with this particular technique were liable to display a variety of defects, including spattering, tapering, microcracks, and recast layer. Shin et al. [7] conducted an experimental investigation for the shallow angle laser drilling of Inconel 718 and concluded the increase in laser power reduced a thickness of the recast layer due to material removal by vaporization. Girardot et al. [8] used a millisecond pulse laser to drill cobalt-based superalloy and found that interface cracking will occur during laser processing. Sezer et al. [9] conducted laser drilling experiments on TBC Nimonic 263 superalloy and concluded that the recast layer and heat-affected zone (HAZ) were thicker with the smaller drilling angles to the surface.

With the development of ultrashort pulse laser technique [10], ultrashort laser drilling has become an international

✉ Wenjun Wang
wenjunwang@mail.xjtu.edu.cn

[1] School of Mechanical Engineering, Xi'an Jiaotong University, Xi'an 710049, China

[2] State Key Laboratory for Manufacturing Systems Engineering, Xi'an Jiaotong University, Xi'an 710054, China

[3] Shaanxi Key Laboratory of Intelligent Robots, Xi'an 710049, China

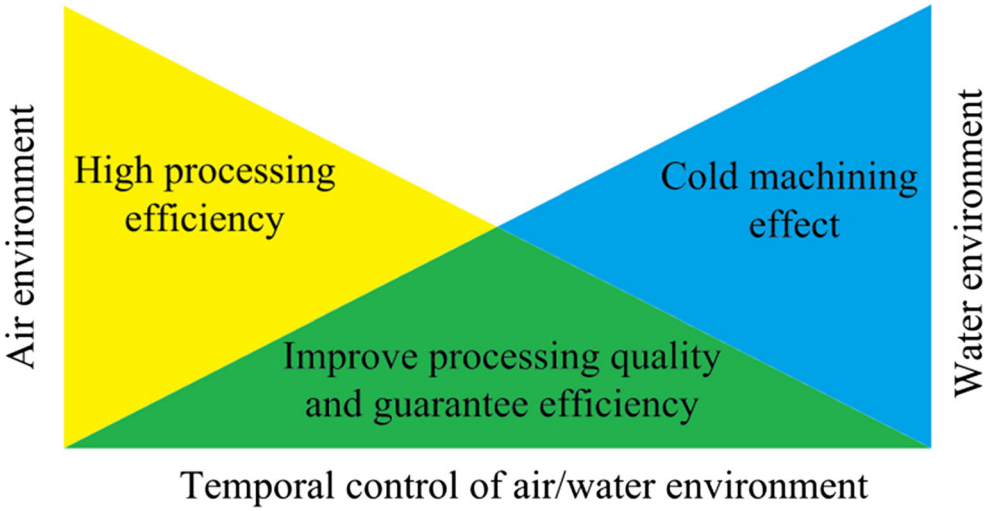

Fig. 1 Schematic diagram of processing characteristic

research hotspot. Ultrashort laser high-precision machining without HAZ has been considered the potential processing technique in the future. However, low efficiency of ultrashort pulse laser processing is the main disadvantage preventing its practical application in industry. The short pulse laser can achieve higher efficiency [11] compared to the ultrashort pulse laser, but the quality of the processing is lower. To improve processing quality of laser drilling, researchers have successively expanded the exploration of laser processing under solution environment [12]. Li et al. [13] reported a chemical assisted laser machining process. It is found that the process improved machining quality compared to that in air. HAZ size and recast have been significantly reduced. It can be concluded that laser ablation under water environment could obviously promote processing quality [14, 15], but processing efficiency is reduced to a certain degree [16]. So, there is limited research on using water environment to combine processing quality and efficiency.

An experimental research of the influence of different processing environments on laser drilling was conducted. By combining characteristics of high processing efficiency under air environment and good quality under water environment, this study proposes the laser processing method with temporal control of air/water environment, since drilling efficiency was not significantly reduced, and cold machining effect of water was applied to improve processing quality. The processing characteristics are shown in Fig. 1.

2 Experimental method

2.1 Materials and methods

This paper was focused on processing microholes on nickel-based alloy with TBCs. The material of the coatings was made with the plasma spraying method. The main compositions of TBC, bond coating layer, and substrate were ZrO_2, NiCrAlY, and Inconel 718 respectively. The heat conductivity of ZrO_2 is the lowest among ceramic materials with the smallest thermal radiation rate, a high reflection rate, and a large coefficient for thermal expansion. The bond coating layer guaranteed tight bonding between the ceramic layer and the substrate. Main chemical compositions of experimental materials are presented in Table 1.

During the experimental procedure, an Inno1316 Nd:YAG diode-pumped solid-state laser produced by INNOLAS was used. HITACHI S-3000N scanning electron microscope (SEM) was utilized to study microhole morphology. OLS4000 laser scanning confocal microscope produced by OLYMPUS was utilized to measure specific dimension of microhole. SU-8010 field emission electron microscope (FEM) produced by HITACHI was applied to conduct energy dispersion spectrum (EDS) analysis.

The experiment light path is shown in Fig. 2; the light beam generated from the laser passed the diaphragm, shutter, and beam splitter successively. The beam splitter divided the light into two directions; one reached power meter and another

Table 1 Main chemical composition list of the sample

Type	Materials	Thickness (μm)	Composition (wt%)					
			Ni	Cr	Al	Fe	Y	ZrO_2
Thermal barrier coating	Zirconia	300						92
Bond coating layer	NiCrAlY	100	67	22	10		1	
Substrate	Inconel 718	2000	55	21	0.8	14		

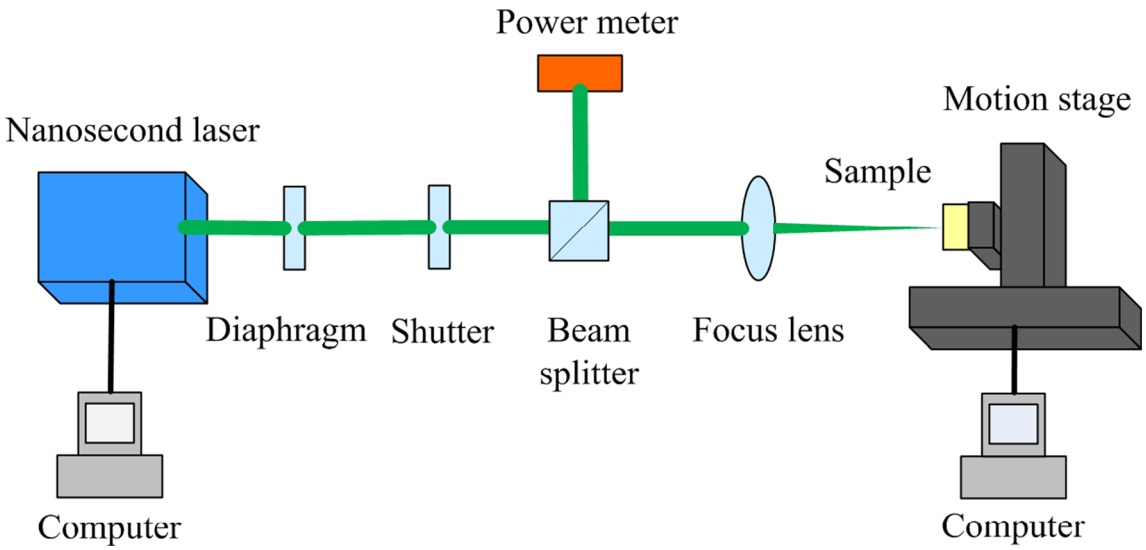

Fig. 2 Light paths in the experiment

reached the experiment material clamped at three-axis motion stage through focusing lens. The nanosecond laser processing parameters used in the experiment are shown in Table 2.

The diameters of the entrance and hole depths were measured with a SEM. The material was split from axis of the hole in order to measure the hole length accurately. The hole depth L was measured from the surface of the TBC to the center of the bottom of the hole. Considering the holes at the entrance may be irregular, the mean value of the minimum and maximum measured values is considered to be an effective value of the diameter. The mean value D_m was calculated by using Eq. (1).

$$D_m = \frac{D_{max} + D_{min}}{2} \quad (1)$$

In this equation, D_{max} is the maximum diameter of the entrance and D_{min} is the minimum of the entrance.

2.2 Experimental classification

Past research demonstrates that laser attenuation [17] in visible wavelength is negligible in pure water. Infrared laser attenuates significantly by wavelength increase; the Nd:YAG solid-state laser (wavelength 1064 nm) attenuates by 60% after 30-mm transport in water. But attenuation of green laser is minimum. Hence, we selected laser with 532-nm wavelength to conduct experimental research. Initially, transmission characteristics of laser in water were analyzed and experimental device is shown in Fig. 3. Water was placed into a quartz flume and a laser power meter was used to measure power value of laser transmission in solution. The thickness of quartz flume was 2 mm.

Table 2 Table of processing parameters

Parameter	Value
Wavelength (nm)	532
Pulse width (ns)	10
Repetition frequency (Hz)	100
Laser power (W)	2.45
Laser mode	TEM_{00} ($M^2 < 1.3$)
Focal length(mm)	150

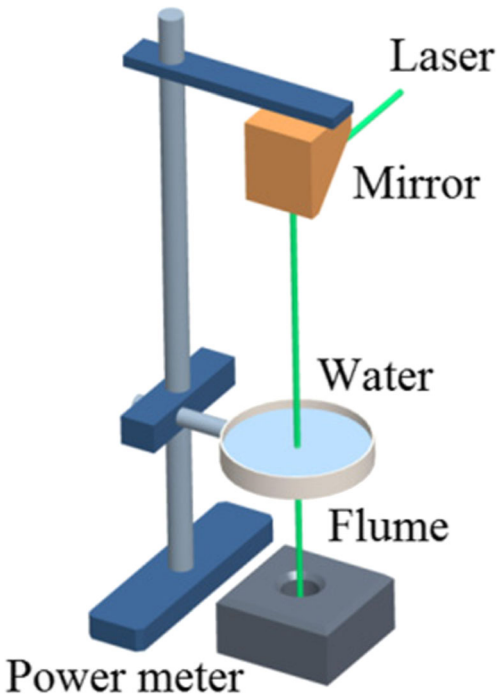

Fig. 3 Experimental scheme of laser power measurement

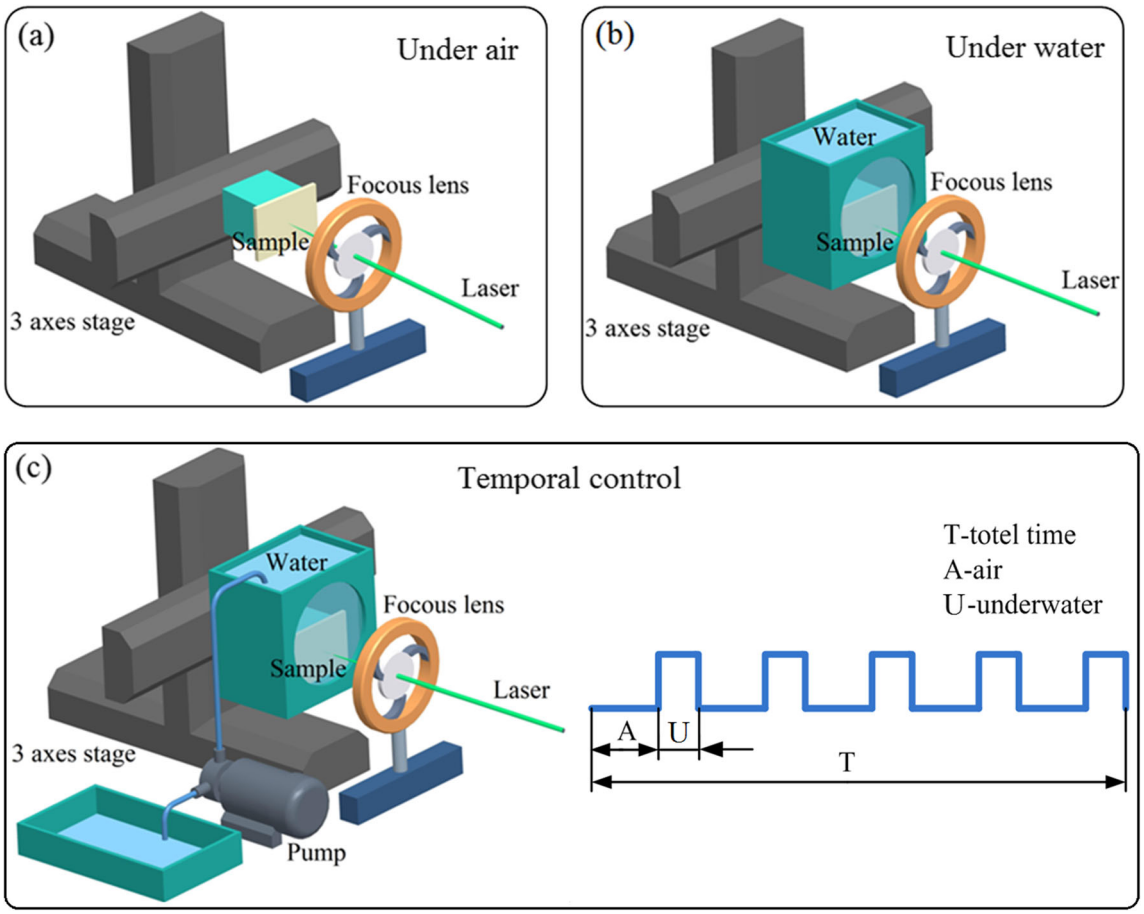

Fig. 4 Experimental scheme of laser drilling: (**a**) under air, (**b**) under water, and (**c**) temporal control

To compare influence of air and water environment on laser process, laser drilling experiments of nickel-based alloy with TBCs are divided into three types:

(a) Laser drilling under air: Focused laser irradiated on sample, which was fixed on motion stage through a support. A computer-adjusted position of motion stage. Experimental device is shown in Fig. 4a.

(b) Laser drilling under water: The sample was fixed in a container with water. Frontage of the container had a quartz window used to irradiate on sample in water. The mounting base of the container was used to adjust the distance from sample to quartz window. The back of the container was designed including mounting hole, used to fix the container and motion stage. Experimental device is shown in Fig. 4b.

(c) Laser drilling of temporal control of air/water environment: A water pump at the side of the container was used. Positive and reverse rotation of water pump controlled the water quantity in the container. Experimental device and the alternation time of processing environment are shown in Fig. 4c. *T* is the total time needed by laser drilling, *A* stands for processing time under air environment, and *U* is the processing time under water environment. While pulses attained 30,000, the processing time *T* reached 5 min. *T* was divided into five equal parts on average, and each part was 1 min. A total of six groups of experiments were conducted. Furthermore, underwater processing time of equal parts increased from 5 to 30 s.

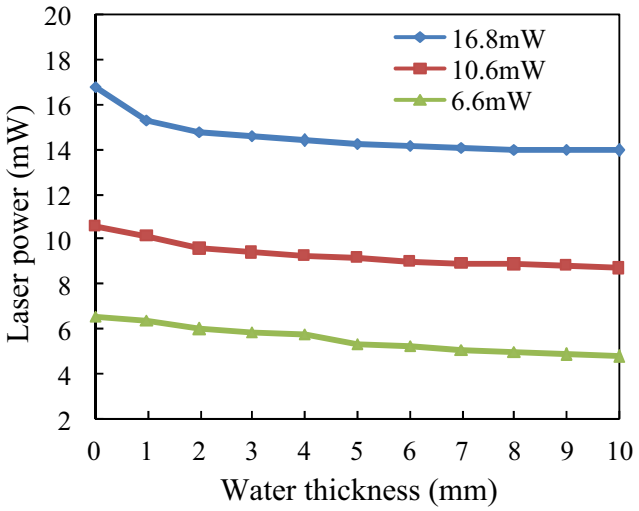

Fig. 5 Attenuation curve of laser power underwater

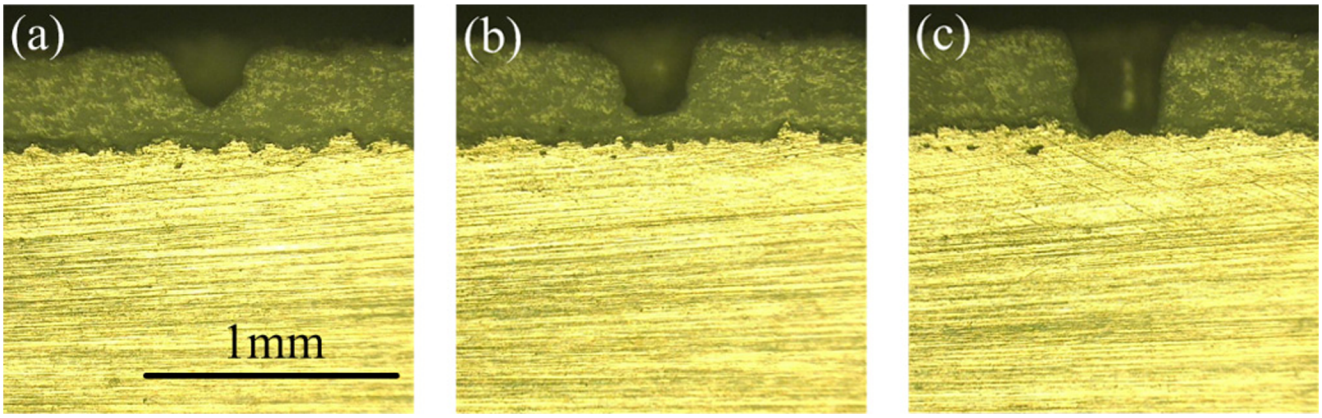

Fig. 6 Profile morphology of laser ablation with different numbers of pulses under air. (**a**) 500, (**b**) 1000, and (**c**) 2000

3 Results and discussion

Laser energy absorbed by water is related to underwater transmission distance. The longer the optical length underwater, the greater the energy attenuation will be and the poorer the processing efficiency will be. Under a certain depth, attenuation degree of underwater laser energy can be solved by Eq. (2) of Beer-Lambert law [18]. This equation was applied to calculate laser energy variation through a certain underwater optical length:

$$I_x(\lambda) = I_0(\lambda)\exp\left(-\frac{x}{\Delta}\right) \quad (2)$$

In this equation, $I_x(\lambda)$ is the light intensity at distance x, $I_0(\lambda)$ is the incident light intensity, x is the distance in solution, and Δ is absorption length of laser in solution.

Experiments were conducted with three different laser powers respectively, since reflection and absorption of water result in certain loss of laser energy. As shown in Fig. 5, it can be concluded that increasing underwater optical length would result in attenuation of laser energy. The absorption lengths of 532- and 1064-nm lasers in pure water are 28.169 m and 29.2 mm [19] respectively. The absorption length was calculated by Eq. (2) based on the experimental dates. The mean value of absorption length of the 532-nm laser under water environment was 22.27 mm. The calculation result was close to the absorption length of the 1064-nm laser in water, but much smaller than the absorption length of the 532-nm laser in published data. Because the thickness of quartz flume used to measure power value of laser transmission was 2 mm, the intensity of laser was attenuated when it passed through the quartz flume.

A series of drilling experiments by applying different numbers of pulses was conducted. The TBC thickness is close to 300 μm; it is pronounced that almost 2000 pulses can remove the TBC under air, as shown in Fig. 6. While the number of pulses required for underwater was nearly twice that of air, the ceramic layer generates heat under the laser beam first during laser processing. The laser will not melt the ceramic layer rapidly because its melting point is as high as 2680 °C. All

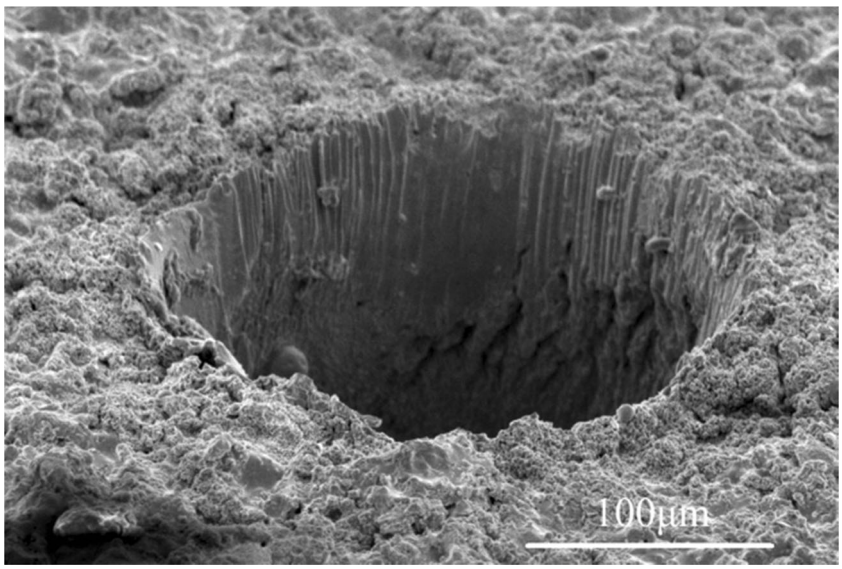

Fig. 7 Entrance morphology of laser ablation with 2000 pulses under air

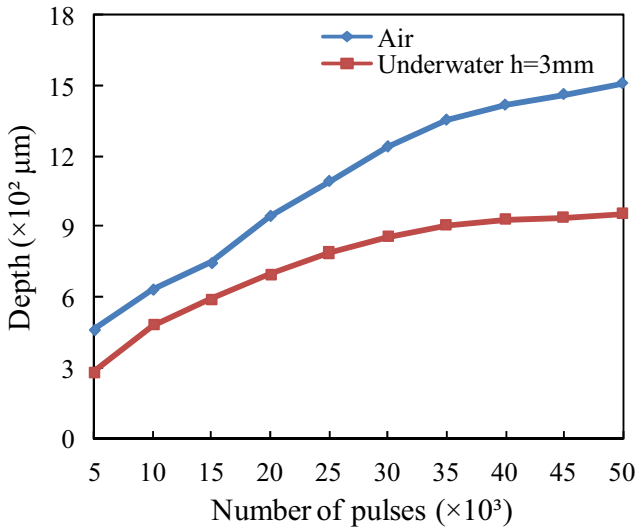

Fig. 8 Microhole depths of laser ablation with different numbers of pulses

heat accumulates in the ceramic layer and transfers to the metal basis. However, the melting point of Inconel 718 is lower, 1290 °C. Since the laser energy at the focal spot is the highest, the TBC of material surface can be effectively removed by laser pulses. The material deposited around the hole entrance is not obvious when the processing depth is shallow, as shown in Fig. 7.

Figure 8 shows that the depth of hole was enlarged as the number of pulses increased. Additionally, in the last few groups of pulse experiments, drilling depth under water environment was not apparently enlarged, tending to be under saturation status. Figure 9 showed the hole diameter formed by increasing the number of laser pulses from 5000 to 50,000. These results showed that hole diameters in laser drilling under different environments expanded as the number of pulses increased. Initially, the tendency was similar, but

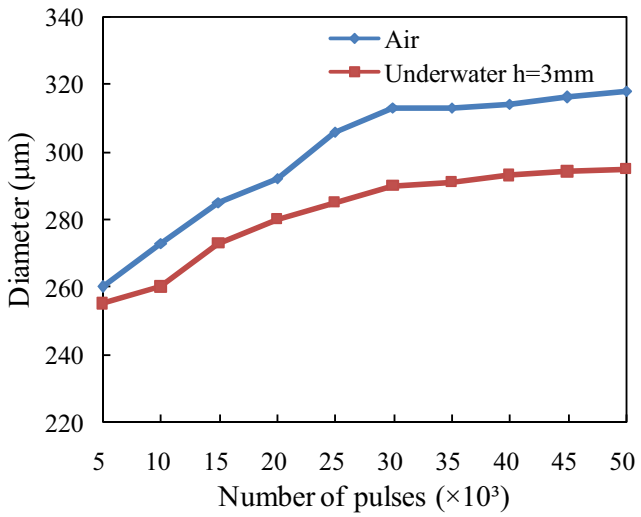

Fig. 9 Microhole diameters of laser ablation with different numbers of pulses

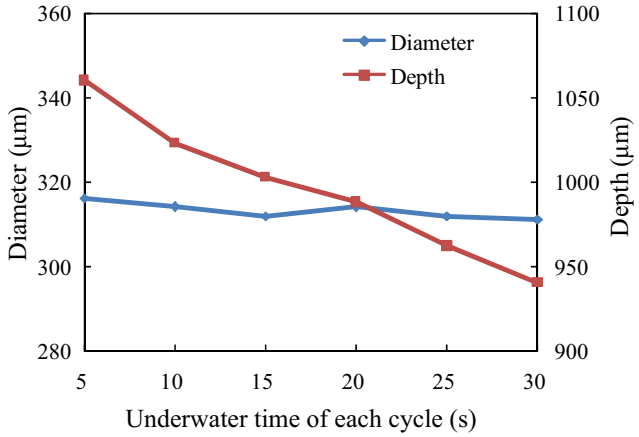

Fig. 10 Microhole diameter and depth of laser ablation under different environmental temporal controls

subsequently, due to the absorption effect of water on laser, laser energy reaching the material surface is reduced, thus weakening the processing effect.

Drilling experiment of temporal control of air/water environment adopted laser parameters similar to those under a single-environment method. The proportion of pulse numbers of underwater in total pulses increased from 1:12 to 1:1. Figure 10 shows the hole diameter and depth variations under different temporal controls. It is found that the hole diameter variation was not significant as underwater processing time prolonged, but hole depth gradually decreased.

A set of results is shown to conduct a detailed comparison of drilling effects. When the laser power was 2.45 W and pulse number was 30,000 in the three types of experiments, underwater time U in temporal control was 5 s and air time A in temporal control was 55 s. The hole diameter and depth were the greatest in air environment and were the least in water environment. The dimensions in temporal control were

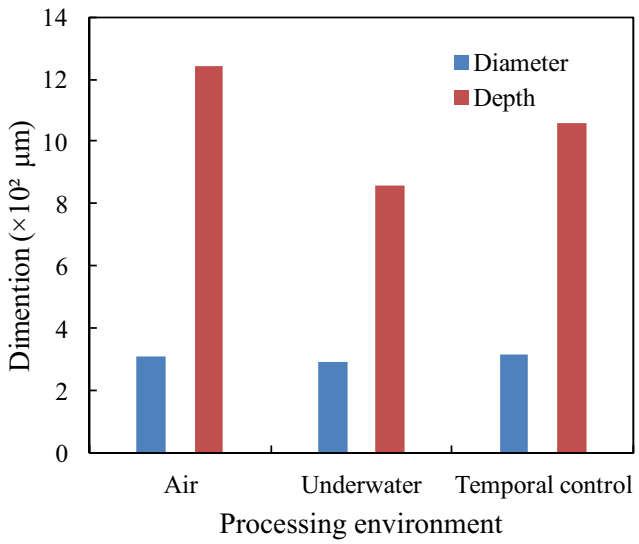

Fig. 11 Microhole diameter and depth of laser ablation under different environments

between the air and water environments. The comparison of hole diameter and depth of three methods with the same processing parameters is shown in Fig. 11.

The morphologies of microhole entrances ablated by laser in different environments are shown in Fig. 12. Figure 12(a) shows entrance morphology of laser drilling under air environment. Figure 12(a1) showed that molten splashes deposited around the entrance obviously, since materials were piled up and formed an annular convex structure. In Fig. 12(a2), ripples formed by laser energy ablation on the hole wall are observed.

Figure 12(b) showed entrance morphology of laser drilling under water environment. In Fig. 12(b1–b2), it is showed that morphology quality of entrance and profile is obviously improved. Roundness and roughness of the hole wall were promoted by a large margin. Water nearby the focus would absorb laser energy with bremsstrahlung through gas vaporization and ionization. Laser plasmas of high temperature and high pressure would be generated within the focusing region. Plasmas expand at supersonic speed continuously compressing surrounding water, thus forming plasma impact waves [20] during pulsation and collapse of cavitation bubble.

Figure 12(c) shows entrance morphology of laser drilling in temporal control of air/water environment. It can be concluded from Fig. 12(c1–c2) that laser drilling in temporal control of air/water environment was improved in quality in comparison with a single environment. There were no materials deposited at entrance and ripples formed on the hole wall were observed. Roundness of microhole and roughness of the hole wall were improved by a large margin.

EDS analyses of different measuring regions of microhole entrance are shown in Fig. 13. Figure 13a, b shows analysis results of point A and point B in Fig. 12(a2). Figure 13c shows analysis results of point C in Fig. 12(b2). Figure 13d shows

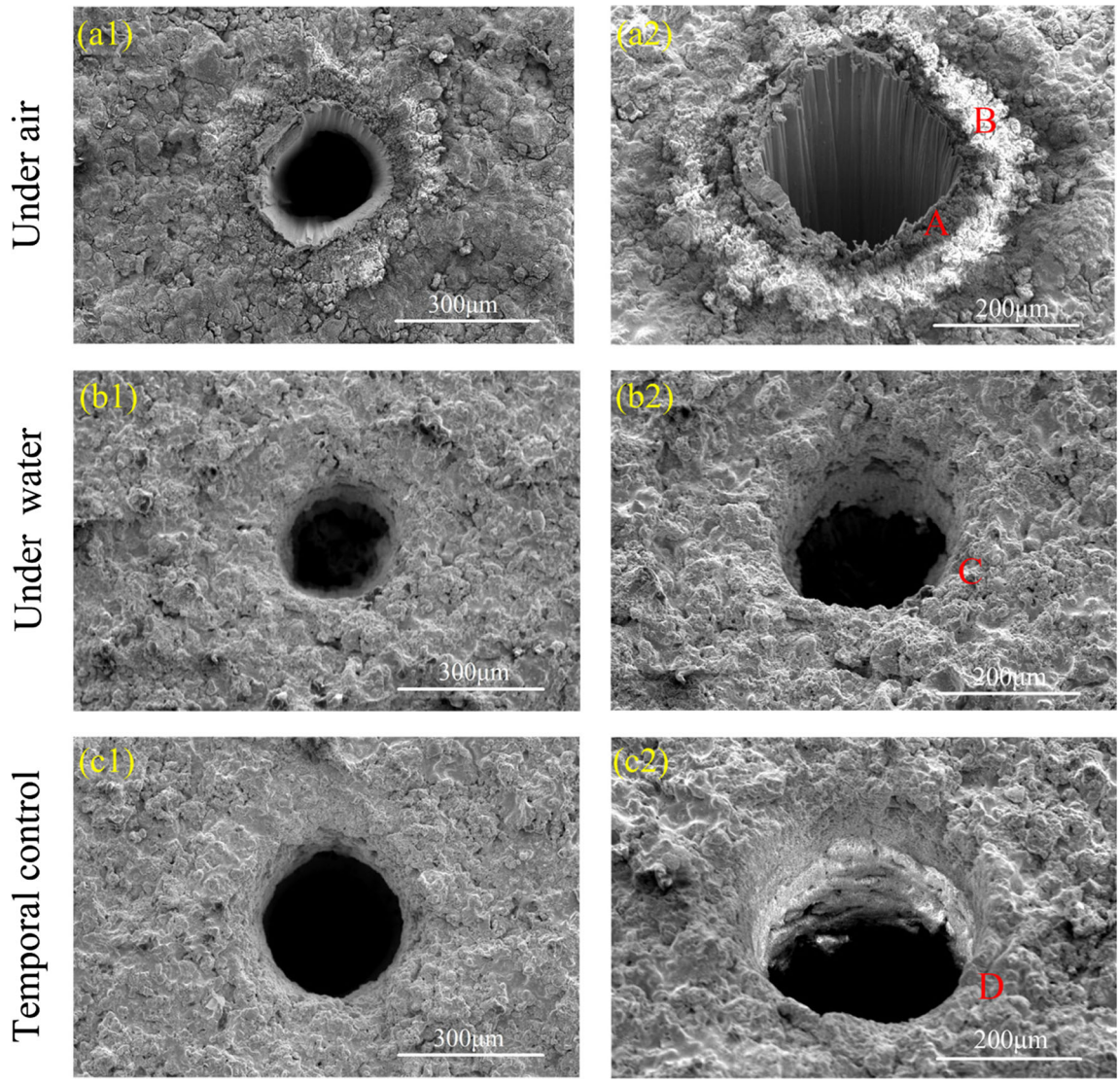

Fig. 12 Microhole entrance morphology of laser ablation under different environments: (**a**1) top view under air, (**a**2) oblique view under air, (**b**1) top view under water, (**b**2) oblique view under water, (**c**1) top view of temporal control, and (**c**2) oblique view of temporal control

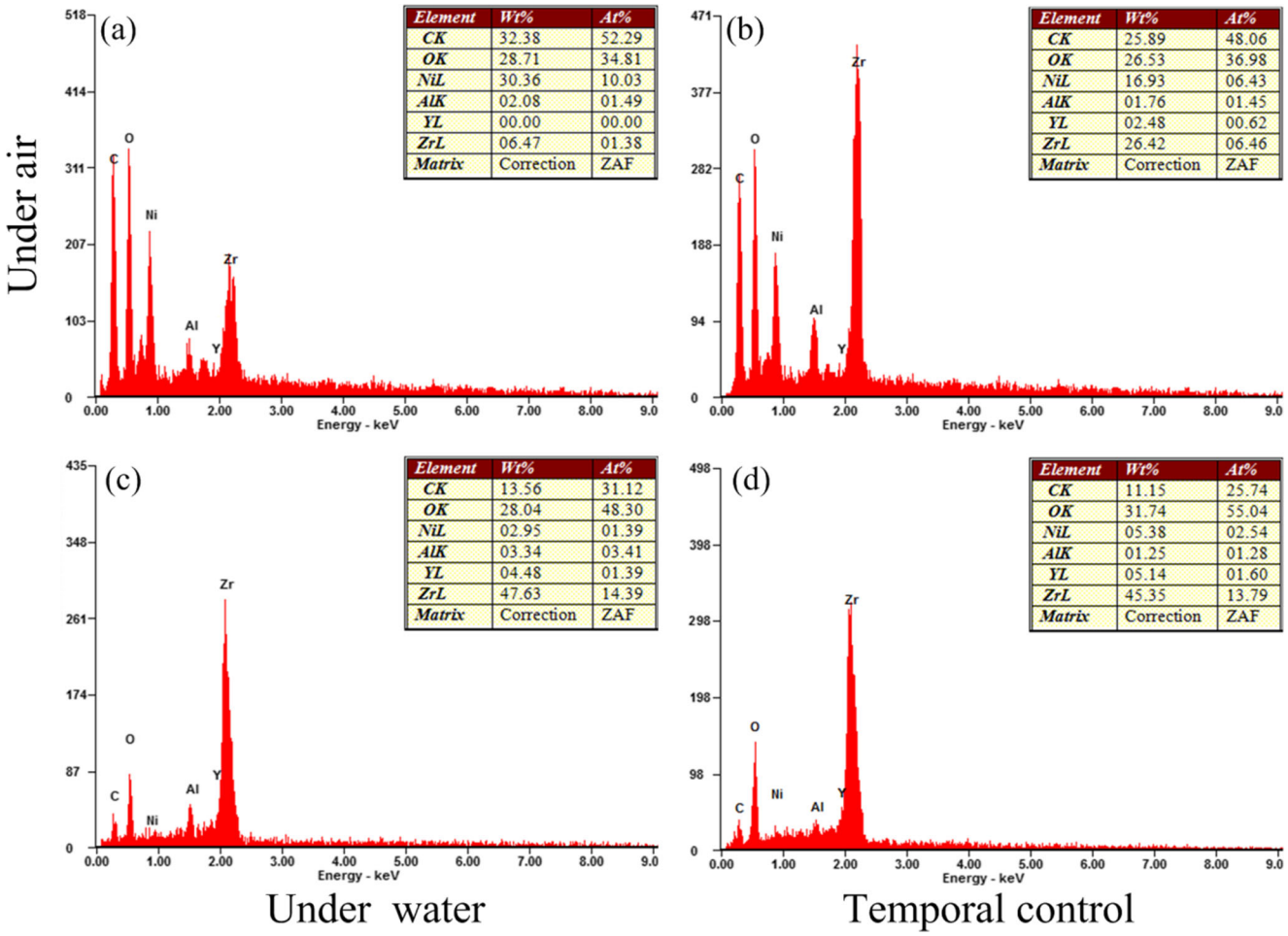

Fig. 13 EDS analysis graph in different measuring regions: (**a**) point A under air environment, (**b**) point B under air environment, (**c**) point C under water environment, and (**d**) point D of temporal control

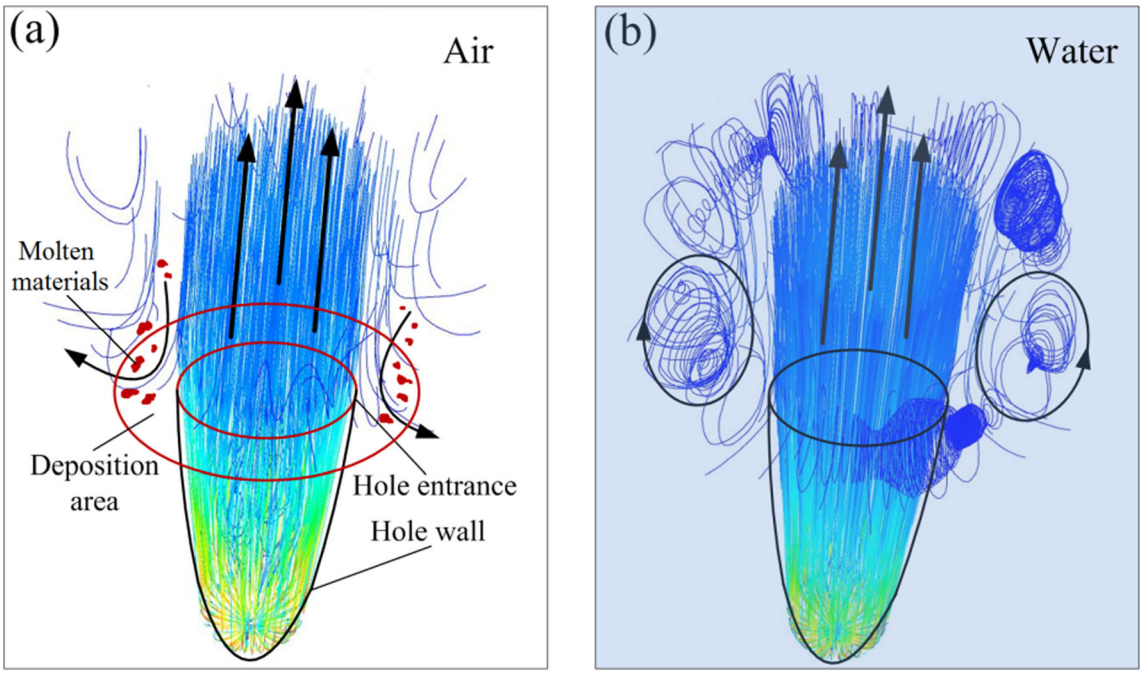

Fig. 14 Schematic diagram of influence of shock wave under different environments: (**a**) air environment and (**b**) water environment

analysis results of point D in Fig. 12(c2). By result comparison, it is showed that due to ionizing of air during laser processing, CO_2 in air was ionized and C element content on material surface increased. The ionization would be stronger at the center of the hole. C element content in region A (C of 32.38 wt%) was higher than that in region B (C of 25.89 wt%), while Ni, Al, and Y in bond coating layer and nickel-based alloy deposited at hole entrance. In the laser processing under temporal control of air/water environment, C element content was apparently lower compared to air environment. Due to the effect of impact waves in water, limited quantity of elements in bond coating layer and nickel-based alloy deposited at entrance. Because the laser processing in temporal control of air/water environment was not completely isolated from the air, element content of Ni and Y which form a bond coating layer and nickel-based alloy in region D (Ni of 5.38 wt%, Y of 5.14 wt%) was higher than that of region C (Ni of 2.95 wt%, Y of 4.48 wt%).

Because the drilling depth has exceeded the thickness of the TBCs, Ni, Al, and Y in the bond coating layer and nickel-based alloy deposited at hole entrance. Therefore, the content of Zr (6.47%) was relatively low. Due to the effect of impact waves in water and temporal control of air/water environment, limited quantity of elements in the bond coating layer and nickel-based alloy deposited at entrance; the original element content of TBC in the measuring region was dominant. Therefore, the content of Zr (45.35%) was relatively high. Figure 14 shows a schematic diagram of influence of shock wave under different environments.

To compare the processing effect under different environments, the materials in Fig. 12 were split from axis of the hole.

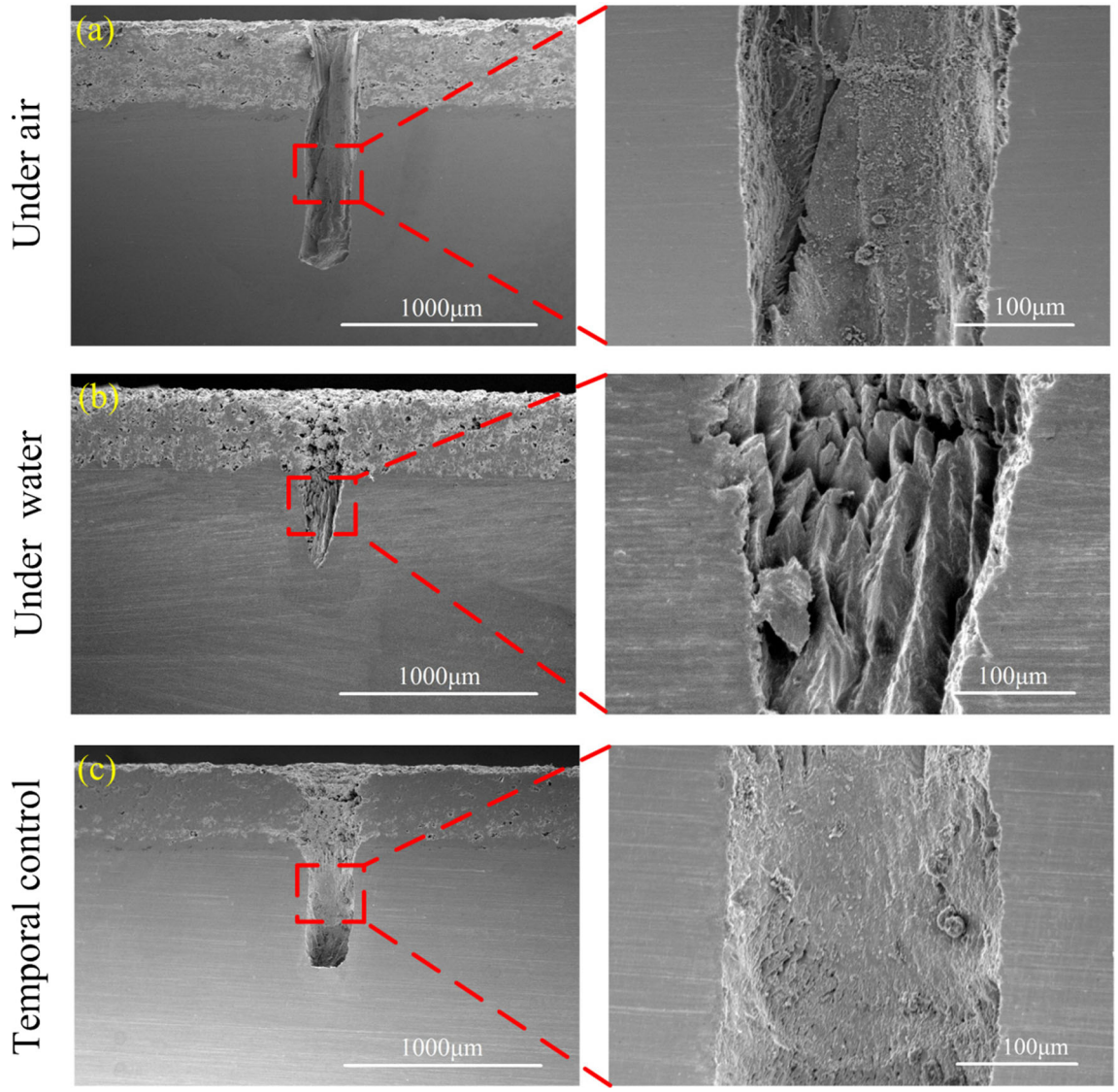

Fig. 15 Microhole sectional morphologies of laser ablation under different environments: (**a**) section view under air, (**b**) section view under water, and (**c**) section view of temporal control

Table 3 Machining effect of laser ablation under different environments

Type	Roughness (μm)	Roundness (μm)	Taper
Under air	24	25	0.17
Under water	61	11	0.51
Temporal control	12	6	0.05

Figure 15 shows side wall morphology comparison. The two groups of SEM results came from the same set of experiments. Figure 15a showed side wall morphology of laser drilling under air environment. It can be concluded that the microhole side wall was covered by a recast layer and longitudinal cracks.

Figure 15b showed side wall morphology of laser drilling of nickel-based alloy with TBCs, under water environment. The recast layer of microhole was removed, and since the density of water was greater compared to that of air, momentum of water of the same volume would be far greater than that of air. Furthermore, the machining effect of water on microhole was stronger than that of air in laser drilling [21]. As the side wall restrained shock wave generated by a cavitation effect in water, significantly, gully erosion appeared at the side wall. The microhole depth of underwater laser drilling was shallow, but the taper of the microhole was relatively large. The absorption of laser energy by water is only one cause of the microhole depth decrease. The laser was focused on the material surface in the three types of experiments, but the location of the material surface radiated by the laser produces quantity of bubbles in water. These bubbles have a significant effect on the reflection and refraction of the laser. Due to the abovementioned, laser energy reaching the surface of material is weakened.

Figure 15c shows side wall morphology of laser drilling in temporal control of air/water environment. Few recast layers on the microhole side wall were observed and the hole wall was relatively smooth. It is showed that cracks and solidified melting particles of the side wall under temporal control of air/water environment were reduced compared with those under air environment. Furthermore, gully erosion effectively disappeared on the side wall compared with those under water environment.

The roundness of hole entrance, the roughness (R_z), and the taper of the hole wall were measured and calculated. Machining effects of laser ablation of three methods are shown in Table 3. Laser drilling of temporal control of air/water environment was improved in quality in comparison with a single environment. Roughness, roundness, and taper of microholes were promoted by a large margin.

By comparing the experimental results, it showed that a proper application of shock wave in water environment can help to improve the roughness of the hole wall and avoid molten splash deposits at the hole entrance, so that the quality of nanosecond laser drilling will be improved. But it is also important to note that reasonable control of underwater processing time was very critical in experiment. When the time of underwater processing is too short, shock wave underwater processing almost had no effect; significantly, cracks and particles formed by high-temperature melting appeared at the side wall. When the time of underwater processing was too long, significantly, gully erosion appeared as the side wall restrained shock wave generated by a cavitation effect in water. And the absorption of laser energy will cause the reduction of processing efficiency. When the underwater time in temporal control was 5 s, cracks and particles formed by high-temperature melting were effectively reduced, and 5 s was also the critical time for the gully generation. So, we concluded that 5 s underwater was the optimum time in the series of experiments. Figure 16 shows comparison of laser processing effects under different environments.

The processed microholes under temporal control showed high roundness and there was no material deposition at entrance. Besides, the taper of the side wall was approximately equal to zero. Compared with the existing research results of laser drilling of TBCs, temporal control of air/water environment can reduce thermal stress effectively in laser drilling due to the cooling effect of water and thus restrain the formation of cracks. So, there were no cracks inside the microhole or

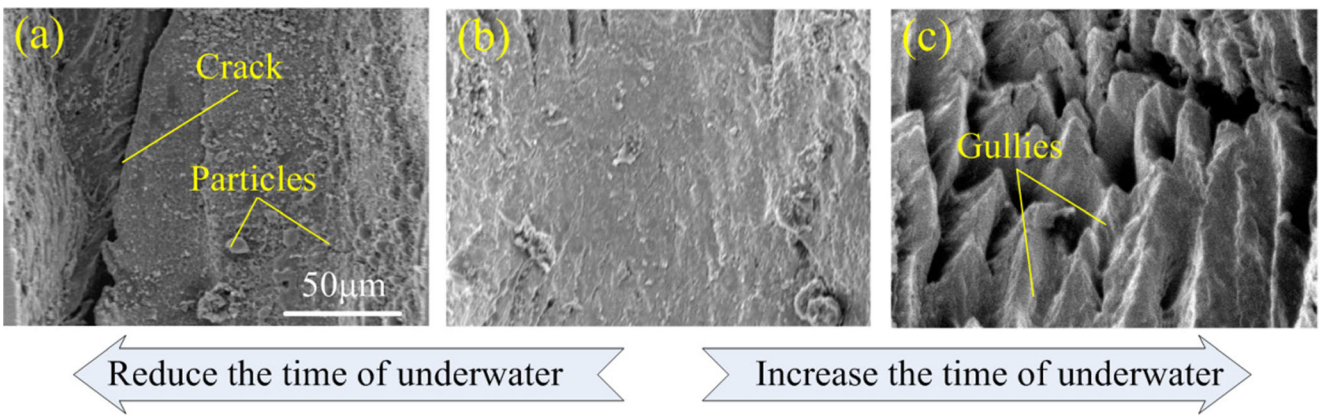

Fig. 16 Comparison of laser processing effects under different environments: (**a**) under air, (**b**) temporal control, and (**c**) under water

between coating and substrate caused by thermal stress [22]. Due to impact waves generated under water environment during pulsation and collapse of cavitation bubble, it would generate impact force on material. Thus, there were no irregular hole shapes caused by melting deposition [23, 24].

4 Conclusions

To compare the influence of different environments on laser processing, we divided drilling experiments of nickel-based alloy with TBCs into three types: (a) laser drilling under air, (b) laser drilling under water, and (c) laser drilling in temporal control of air/water environment. The following conclusions were drawn through experiments. Since impact waves generated under water environment during pulsation and collapse of cavitation bubble, it would generate impact force on material. But a sustaining impact effect formed significantly during gully erosion appears on the side wall. Laser drilling of temporal control of air/water environment was improved in quality in comparison with a single environment. No obvious cracks and other defects were observed. Roundness, roughness, and taper of microholes were promoted by a large margin. Temporal control of air/water environment used impact wave generated by laser in water. Therefore, the temporal control combined advantages of traditional laser drilling under air and water, and processing efficiency is guaranteed with quality improvement.

Funding information This work was supported by the National key R&D Program of China (grant no. 2016YFB1102502), the National Natural Science Foundation of China (grant nos. 51475361, 91323303, and 51421004), and the Program for Changjiang Scholars and Innovative Research Team in University (grant no. IRT_15R54).

References

1. Guo YF, Zhang GW, Wang L, Hu YH (2016) Optimization of parameters for EDM drilling of thermal-barrier-coated nickel superalloys using gray relational analysis method. Int J Adv Manuf Technol 83:1595–1605
2. Zhang Y, Xu ZY, Zhu D, Qu NS, Zhu Y (2016) Drilling of film cooling holes by a EDM/ECM in situ combined process using internal and side flushing of tubular electrode. Int J Adv Manuf Technol 83:505–517
3. Fan ZJ, Dong X, Wang KD, Duan WQ, Wang RJ, Mei XS, Wang WJ, Cui JL, Yuan X, Xu CY (2016) Effect of drilling allowance on TBC delamination, spatter and re-melted cracks characteristics in laser drilling of TBC coated superalloys. Int J Mach Tool Manu 106:1–10
4. Imran M, Mativenga PT, Gholinia A, Withers PJ (2015) Assessment of surface integrity of Ni superalloy after electrical-discharge, laser and mechanical micro-drilling processes. Int J Adv Manuf Technol 79:1303–1311
5. Zhang H, Xu JW (2012) Laser drilling assisted with jet electrochemical machining for the minimization of recast and spatter. Int J Adv Manuf Technol 62:1055–1062
6. Chien WT, Chin SH (2007) Investigating the recast layer formed during the laser trepan drilling of Inconel 718 using the Taguchi method. Int J Adv Manuf Technol 33:308–316
7. Shin J, Mazumder J (2017) Shallow angle drilling of inconel 718 using a helical laser drilling technique. J Manuf Sci Eng 139: 031004
8. Girardot J, Schneider M, Berthe L, Favier V (2013) Investigation of delamination mechanisms during a laser drilling on a cobalt-base superalloy. J Mater Process Technol 213:1682–1691
9. Sezer HK, Li L (2009) Mechanisms of acute angle laser drilling induced thermal barrier coating delamination. J Manuf Sci Eng 131: 051014
10. Zhai ZY, Wang WJ, Zhao J, Mei XS, Wang KD, Wang FC, Yang HZ (2017) Influence of surface morphology on processing of C/SiC composites via femtosecond laser. Compos Part A 102:117–125
11. Döring S, Szilagyi J, Richter S, Zimmermann F, Richardson M, Tünnermann A, Nolte S (2012) Evolution of hole shape and size during short and ultrashort pulse laser deep drilling. Opt Express 20: 27147–27152
12. Nath AK, Hansdah D, Roy S, Choudhury AR (2010) A study on laser drilling of thin steel sheet in air and underwater. J Appl Phys 107:551–117
13. Li L, Achara C (2004) Chemical assisted laser machining for the minimisation of recast and heat affected zone. CIRP Ann Manuf Technol 53:175–178
14. Zhang DS, Gökce B, Sommer S, Streubel R, Barcikowski S (2016) Debris-free rear-side picosecond laser ablation of thin germanium wafers in water with ethanol. Appl Surf Sci 367:222–230
15. Iwatani N, Doan HD, Fushinobu K (2014) Optimization of near-infrared laser drilling of silicon carbide under water. Int J Heat Mass Tranf 71:515–520
16. Choo KL, Ogawa Y, Kanbargi G, Otra V, Raff LM, Komanduri R (2004) Micromachining of silicon by short-pulse laser ablation in air and under water. Mater Sci Eng A 372:145–162
17. Li BH, Zhao JS, Yuan LX, Zhang H, Xu JW (2010) Basic research on properties of green laser machining in water. Mach Build Autom (in Chinese) 39:47–49
18. Kruusing A (2004) Underwater and water-assisted laser processing: part 1-general features, steam cleaning and shock processing. Opt Lasers Eng 41:307–327
19. Hale GM, Querry MR (1973) Optical constants of water in the 2002 nm to 2002 μm wavelength region. Appl Opt 12:555–563
20. Zhou ZH, Li XH, Xie CX, Zhu M, Feng J (2016) Silicon surface topography by laser-induced plasma shock waves in the air and under water. Laser Optoelectron Prog (in Chinese) 10:216–225
21. Zhai ZY, Wang WJ, Mei XS, Wang KD, Yang HZ (2017) Influence of plasma shock wave on the morphology of laser drilling in different environments. Opt Commun 390:49–56
22. Sezer HK, Li L, Schmidt M, Pinkerto AJ, Anderson B, Williams P (2006) Effect of beam angle on haz, recast and oxide layer characteristics in laser drilling of tbc nickel superalloys. Int J Mach Tool Manu 46:1972–1982
23. Bathe R, Padmanabham G (2014) Evaluation of laser drilling of holes in thermal barrier coated superalloys. Mater Sci Technol 30: 1778–1782
24. Voisey KT, Clyne TW (2004) Laser drilling of cooling holes through plasma sprayed thermal barrier coatings. Sur Coat Technol 176:296–306